AGU PUBLICATIONS

Geophysical Research Letters

RESEARCH LETTER
10.1002/2016GL071768

Key Points:
- Droughts can displace hundreds of kilometers from their origin
- Several regions experience high mobility and consistent displacement patterns of droughts
- Droughts tend to lock into further growth and intensification after reaching a certain area and intensity

Supporting Information:
- Supporting Information S1

Correspondence to:
J. E. Herrera-Estrada,
jherrera@princeton.edu

Citation:
Herrera-Estrada, J. E., Y. Satoh, and J. Sheffield (2017), Spatiotemporal dynamics of global drought, *Geophys. Res. Lett.*, *44*, 2254–2263, doi:10.1002/2016GL071768.

Received 1 NOV 2016
Accepted 7 FEB 2017
Accepted article online 18 FEB 2017
Published online 4 MAR 2017

Spatiotemporal dynamics of global drought

Julio E. Herrera-Estrada[1], Yusuke Satoh[2], and Justin Sheffield[1,3]

[1]Department of Civil and Environmental Engineering, Princeton University, Princeton, New Jersey, USA, [2]International Institute for Applied Systems Analysis, Laxenburg, Austria, [3]Geography and Environment, University of Southampton, Southampton, UK

Abstract Understanding the evolution and physical drivers of drought is critical to informing forecasting efforts. One aspect that has seldom been explored is the joint evolution of droughts in space and time. Most studies fix the reference area and focus on their temporal variability or study their spatial heterogeneity over fixed durations. This work implements a Lagrangian approach by aggregating contiguous areas under drought into clusters. These clusters become the frame of reference and are tracked as they evolve through space and time. Clusters were identified from soil moisture data from the Climate Forecast System Reanalysis (1979–2009). Evapotranspiration, moisture fluxes, and precipitation were used to explore the relevance of possible mechanisms of drought propagation. While most droughts remain near their origin, the centroid of 10% of clusters traveled at least 1400–3100 km, depending on the continent. This approach also revealed that large-scale droughts often lock into further growth and intensification.

Plain Language Summary Droughts are some of the most expensive natural disasters that society has to face, so understanding how they evolve and what are the physical mechanisms that control them is critical for improving our ability to predict them. Past research has focused mostly on how droughts evolve in time over a fixed region and how droughts of a given duration evolve in space. However, little work has been done to study how they evolve in time and space, simultaneously, leading to a significant gap in our understanding of these extreme events. In this work we identify individual drought events between 1979 and 2009 around the world and track them in space and time to analyze their characteristics and behaviors across different continents. We find that some droughts can travel hundreds of kilometers from where they originated (e.g., from the U.S. Southwest to the U.S. Midwest), and that after droughts have grown and become intense enough, they will tend to become even larger and more intense before conditions improve (i.e., conditions will tend to become worse before they become better).

1. Introduction

Droughts can be deadly and extremely costly [*Sheffield and Wood*, 2011]. Continuous study of these hazards has allowed us to improve our ability to forecast them and develop early warning systems that provide useful information to agricultural, energy, water, and humanitarian aid sectors. However, we have still failed to predict important droughts, like the one that struck the U.S. Great Plains in the summer of 2012 [*Hoerling et al*., 2014] and contributed to increases in global food prices [*World Bank*, 2012]. This is partly because we do not yet fully understand how droughts arise, persist, evolve, and recover [*Wood et al*., 2015]. A contributing factor is how we characterize and analyze droughts' spatiotemporal dynamics from observations or model predictions.

Previous studies often reduce drought analysis from three dimensions (i.e., latitude, longitude, and time) to one or two [*Lloyd-Hughes*, 2012]. Most have focused on time series analysis of area-averaged variables [see *Mishra and Singh*, 2011, for a review], ignoring conditions in the immediate surroundings of the arbitrary domains and over upwind regions that are connected to the areas of interest through atmospheric circulation patterns. Few recent studies have analyzed how droughts evolve simultaneously in space and time, by tracking drought clusters—i.e., spatially contiguous areas under drought—and analyzing their characteristics. *Andreadis et al*. [2005] introduced an innovative clustering algorithm to track droughts through space and time along their duration. They used it to introduce severity-area-duration (SAD) curves for the U.S. to assess the spatial variability of droughts of set durations. However, they did not focus on the monthly dynamics themselves. Later studies replicated the SAD curve analysis globally [*Sheffield et al*., 2009] and for other regions [e.g., *Zhan et al*., 2016]. Some studies at the country [e.g., *Vicente-Serrano*, 2006; *Vidal et al*., 2010; *Xu et al*., 2015; *Zhai et al*., 2016] and continental [*Lloyd-Hughes*, 2012] scales have explored drought

cluster characteristics (e.g., distribution of centroids, direction of displacement over time, and changes in cluster area, intensity, and severity). However, the regional scale of these studies still bounds the frame of analysis and prevents a thorough comparison of the spatiotemporal characteristics of drought across the globe. Furthermore, previous studies have been limited to simple assessments of the time series of drought area and intensity [*Vicente-Serrano*, 2006; *Vidal et al*., 2010; *Gocic and Trajkovic*, 2014; *Wang et al*., 2015], or report aggregate regional drought statistics that do not provide insight into the behavior of individual events [*Tallaksen and Stahl*, 2014; *Ge et al*., 2016].

While the initial onset of droughts is hard to predict, given that it often stems from random atmospheric variability and long-range teleconnections from climatic oscillations [e.g., *Rajagopalan et al*., 2000; *Giannini et al*., 2003; *Shabbar and Skinner*, 2004; *Mo and Schemm*, 2008; *Wu and Kinter*, 2009], local and regional feedbacks with the land surface can play a larger role in the subsequent evolution of droughts. Land-atmospheric feedback mechanisms, such as precipitation recycling [e.g., *Rodriguez-Iturbe et al*., 1991a, 1991b; *Eltahir and Bras*, 1996], have been linked to the intensification and persistence [*Giannini et al*., 2003; *Wu and Kinter*, 2009; *D'Odorico et al*., 2013; *Roundy et al*., 2013] and even propagation of droughts within a continent [*Dominguez et al*., 2009; *Sheffield et al*., 2009; *Sheffield and Wood*, 2011]. Thus, in order to understand better how droughts evolve within a region, it is also important to take into account its surroundings and the regions to which it is atmospherically connected. This can be achieved by carrying out joint spatiotemporal analysis of droughts that provides a more complete picture of their development beyond their origin. Increased understanding of the relevant local and regional land-atmospheric feedbacks, which this approach would bring, may inform the physical processes that need to be improved in climate models to help advance predictive capabilities.

Here we use a Lagrangian approach where individual drought events become the frame of reference, providing unique insights into the spatiotemporal dynamics of droughts. Several characteristics of drought behavior are proposed and analyzed, including how droughts displace across continents and their monthly patterns of growth, intensification, and recovery. The statistics of these characteristics are aggregated to the continental scale and compared globally to evaluate regional differences in drought behavior. Droughts are defined based on soil moisture from reanalysis data. Furthermore, to study the extent to which drought displacements occur downwind through reductions of moisture exports, anomalies in evapotranspiration (ET), moisture fluxes (MF), and precipitation (Prcp) along the clusters' tracks are analyzed. We hypothesize that the drought dynamics analyzed here are driven by a combination of atmospheric drivers, land-atmosphere feedbacks, and geographic factors, including merging and splitting of individual droughts. In this study, we explore the spatiotemporal characteristics of droughts in a systematic way as a first step to understanding the mechanisms of their development, persistence, and displacement.

2. Material and Methods

We used data from the Climate Forecast System Reanalysis (CFSR) to identify areas under drought using a percentile threshold definition. Contiguous regions under drought were aggregated into clusters and tracked over time and space. Characteristics of the clusters were calculated and compared across continental regions.

2.1. Data and Definitions

Monthly 2 m soil moisture, Prcp, latent heat flux, and tropospheric (1000 mbar–250 mbar) wind and specific humidity data from CFSR at 0.5° resolution from 1979 to 2009 were used. Latent heat flux was used as a proxy for evapotranspiration, so it is referred to as ET henceforth. CFSR is a state-of-the art reanalysis that has been used for land-surface hydrology research [e.g., *Mo et al*., 2011; *Meng et al*., 2012] and has been identified to generally reproduce observed droughts more accurately than other reanalysis data sets [*Zhan et al*., 2016]. We focus on agricultural droughts calculated from soil moisture, given its importance for vegetation, agricultural productivity, and for controlling relevant land-atmospheric interactions [*Seneviratne et al*., 2010].

For each variable, percentiles are first calculated from the empirical cumulative distribution function of each month. Individual values are replaced by their respective percentiles, and droughts are defined when these are under a given threshold. The 15th percentile was chosen since it approximates the threshold of common drought metrics, like the Standardized Precipitation Index or Palmer Drought Severity Index value of −1

[*Guttman*, 1999; *Szép et al*., 2005]. This definition allows a direct comparison of dry anomalies across regions with different climates, permitting the study of drought dynamics throughout each continent. This could not be done by using an absolute value threshold.

Drought metrics used here are defined in equations (1)–(3):

$$I_j(t) = 1 - P_j(t) \tag{1}$$

$$\bar{I}(t) = \frac{1}{n}\sum_{j=1}^{n} I_j(t) \tag{2}$$

$$S = \sum_{t=1}^{D} \bar{I}(t) \tag{3}$$

where $I_j(t)$ is the intensity during month t in grid cell j, $P_j(t)$ is the percentile during month t in grid cell j, $\bar{I}(t)$ is the mean intensity of a cluster during month t, n is the number of grid cells in the cluster at time t, S is the cluster's severity, and D is the cluster's duration. Intensity is defined such that lower percentiles represent higher intensities. Sensitivity analyses of the results to the record length and the choice of percentile threshold can be found in Texts S1 and S2 of the supporting information, respectively.

2.2. Clustering Algorithm

The clustering methodology follows *Andreadis et al*. [2005]. After percentiles are calculated and the threshold is implemented at each grid cell, a 2-D median filter is applied to each monthly map to smooth out spatial noise. Contiguous grid cells under drought are then aggregated into clusters. Clusters smaller than 200,000 km^2 are filtered out following *Andreadis et al*. [2005] and *Sheffield et al*. [2009], focusing the analysis on large-scale droughts that have higher likelihood of persisting and displacing. The cluster centroids are found using a weighted center of intensity where the intensity values of the cluster grid cells are used as weights.

Drought events were tracked through time by searching for overlapping grid cells between clusters at contiguous time steps. The tracking algorithm records if a cluster splits, merges, or does both at the same time. Droughts over Greenland, and those whose centroids fell within the Sahara Desert (20°N–25°N, 17°W–34°E) were removed from the analysis, since droughts in these regions were not of interest for this study. Clusters were allowed to propagate into the Sahara until their centroids fell within the described domain.

2.4. Spatial and Statistical Analysis

The drought cluster centroids generate tracks throughout the continents as they displace from month to month. To understand the characteristics of these tracks and whether there are certain regions that experience higher drought displacement, a map of 10-by-10° grid cells was generated, and the number of tracks within each grid cell was counted. For a sensitivity analysis of this resolution choice see the supporting information Text S3. By calculating the number of tracks within these larger grid cells, we obtain a better representation of regions with frequent drought clusters displacing through them. Only monthly displacements with magnitude of 150 km or more were considered to avoid counting small displacements that would fall within the uncertainty of the cluster centroid location. Instances when clusters merged or split were ignored because these result in large changes in the centroid's location. Furthermore, the displacement vector of unit length of each drought cluster was recorded each time a cluster passed through one of these grid cells. The centroids' displacements were also sorted into three categories: (1 and 2) displacement due to asymmetric growth or shrinkage and (3) displacement of the entire cluster. To categorize centroid displacements, the overlap in the number of grid cells in a cluster between two time steps was calculated. If the overlap was equal or larger than 75%, the cluster was considered to have grown or shrunk asymmetrically. This distinction was determined by comparing the cluster areas between time steps. Otherwise, the cluster was determined to have moved locations.

Seven cluster characteristics were evaluated: (1) duration, (2) distance between cluster centroids at the start and at subsequent time steps (i.e., monthly displacement), (3 and 4) cluster areas and mean intensities (equation (2)) at each time step, (5) cluster severity at each time step (equation (3)), and (6 and 7) rate of change in cluster area and mean intensity between time steps. These represent a range of different drought characteristics and dynamics.

Characteristics 1–5 were calculated at every time step for each cluster, and their statistics were aggregated for six continental regions (North America, South America, Europe, Africa, Asia, and Australia). For each region, the complementary conditional distribution functions (CCDF) of the clusters' displacement, maximum area, and severity reaching at least a given threshold value conditional on a range of durations were calculated. The two chosen thresholds values corresponded to the means across regions of the 50th and 80th percentiles of each characteristic for droughts that had lasted 2 years or less (since observations decreased in several regions for longer-lasting clusters). The median durations of clusters that reached a range of displacements were also calculated. The distributions of these characteristics and their comparison between regions can be found in Text S4 of the supporting information.

For each region, the rates of change in area were calculated each month as a function of cluster area in the previous month. Instances when clusters merged or split were discarded, since this often caused large area changes. A 2-D histogram was generated from the scatterplot of rates of change in area against cluster area in the previous month, with 10 bins dividing each axis. Linear regressions were calculated to model how rates of change in area vary as a function of cluster area. This was repeated to model the rates of change in mean intensity as a function of the clusters' mean intensities in the previous month.

A possible mechanism of drought propagation is the reduction of MF downwind caused by reduced ET over an area under drought. This reduction of moisture exports can then lead to decreased Prcp over a region downwind [*Dominguez et al*., 2009]. To do a first approximation of the relevance of this mechanism, vertically integrated MF (1000 mbar–250 mbar) were calculated from monthly data.

To find pairs of regions that have been under drought and are atmospherically connected, disjoint domains R1 and R2 occupied by the same drought cluster at two different points in time t_1 and t_2 ($t_1 < t_2$), respectively, were identified. A linear boundary was drawn at the midpoint between the centroids of R1 and R2 (see Figure 4a), and the length of the boundary was set to the diameter of a circle with an area equal to the mean of the areas of the two domains. The MF perpendicular to the boundary in the direction from R1 to R2 was calculated for every month between 1979 and 2009. If this was positive, then R2 was determined to be downwind from R1. For these cases, Spearman's rank correlations ρ were calculated between monthly time series (1979–2009) of ET anomalies averaged over R1 and the time series of MF anomalies crossing the boundary toward R2, and between the time series of MF anomalies and the time series of Prcp anomalies averaged over R2. If this pair of correlations was positive and statistically significant ($p < 0.05$), the reduction of moisture exports was determined to be a contributing mechanism (but not necessarily the only one) to the propagation of that cluster. This was repeated for each cluster by finding R1 and R2 using $t_1 = 0$ and $t_2 = 2D/3$, and $t_1 = D/3$ and $t_2 = D$, where D is the cluster's total duration, and making sure there was no overlap between any combination of domains.

3. Results

3.1. Spatial Patterns of Drought Displacement

A total of 1420 drought clusters were identified, and their centroids were tracked throughout the world. Figure 1a shows selected contours and the track of an example cluster that displaced from California to the U.S. Great Plains. Figure 1b shows the tracks of drought clusters over North America that lasted at least 3 months and traveled at least 500 km. A map of the track densities in an upscaled grid of 10-by-10° was generated and is displayed in Figure 1c. This shows "hot spots" of cluster tracks in the southeast of the United States, northwest of Mexico, northwest of Brazil, south of Brazil and north of Argentina, central and eastern Europe, central Africa, northwest of India, Southeast Asia, and Australia. These areas cover tropical, temperate, and semiarid climates, suggesting that there are a variety of factors involved in drought displacement within each region. Note that despite some regions experiencing prolonged drought between 1979 and 2009 (e.g., the Sahel), these droughts are not necessarily frequently mobile. This is potentially because atmospheric pressure patterns in these regions are more stable and because these regions may not be important sources of moisture for other areas downwind, preventing the drought signal from propagating farther through reduced moisture exports [e.g., *Giannini et al*., 2003; *Keys et al*., 2014; *Arnault et al*., 2016].

Figure 1c also shows a vector field of the drought clusters' net displacement for each 10-by-10° grid cell. Longer arrows indicate that several clusters followed the same direction. Conversely, short arrows or their

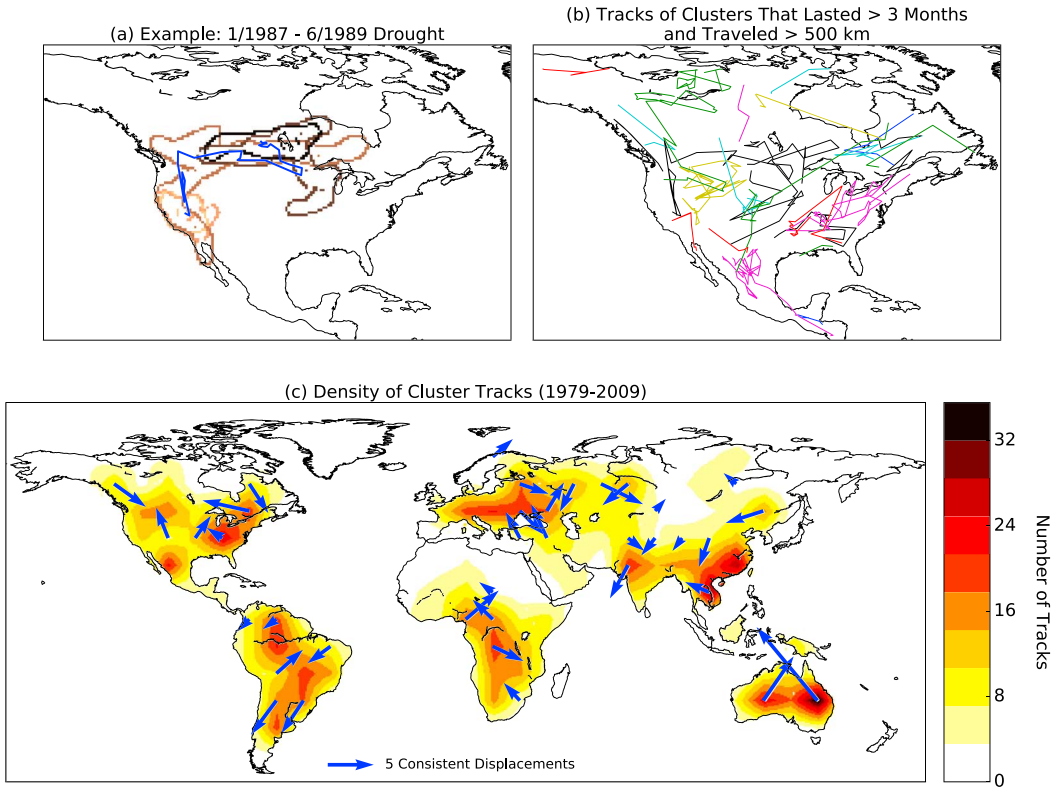

Figure 1. (a) Example of a soil moisture drought cluster. Darker contours show later domains occupied by the cluster. The blue line represents the cluster centroid's track. (b) Drought cluster tracks that displaced at least 500 km and lasted at least 3 months over North America. (c) Density of tracks around the world. Blue arrows represent net direction of droughts passing through.

absence indicates that there were no regional coherent displacement patterns (e.g., clusters moved eastwards almost as frequently as they moved westwards). The longest arrows are found in South America and Australia. For Europe, the lack of arrows is partially due to the smaller number of droughts in the region given the continent's smaller size.

Depending on the region, asymmetric growth was responsible for 10–23% of centroid displacements, asymmetric shrinkage for 13–32%, and cluster displacement for 49–76%. Asymmetric shrinking is more frequent than asymmetric growth since storms can quickly relieve a section of the cluster from drought conditions [e.g., *Kam et al.*, 2013]. Europe and Australia experience the highest proportion of cluster displacement (76% and 58%, respectively); North America and Asia the highest proportion of asymmetric growth (23% and 22%, respectively); and North America, South America, and Africa of asymmetric shrinkage (25%, 25%, and 32%, respectively). The patterns of motion in Figure 1c combine the direction that droughts follow when they displace as well as the direction in which they grow and shrink. As droughts shrink, their centroid may move in the opposite direction in which they grew, suggesting that these displacements could be analyzed further based on the season and the timing of the drought, though the lack of samples makes this challenging.

3.2. Spatiotemporal Characteristics

Figures 2a–2f display the CCDF of displacement, maximum area, and severity reaching at least two different thresholds, conditional on a range of cluster durations for each region. Australian, South American, and European clusters have higher probabilities of displacing further for each duration, while African and North American clusters tend to be more static in comparison. South American and European clusters also have higher probabilities of growing beyond 1 and 2×10^6 km^2, while North American, African, and Australian droughts tend to be smaller. Most regions display similar probabilities of clusters reaching the given

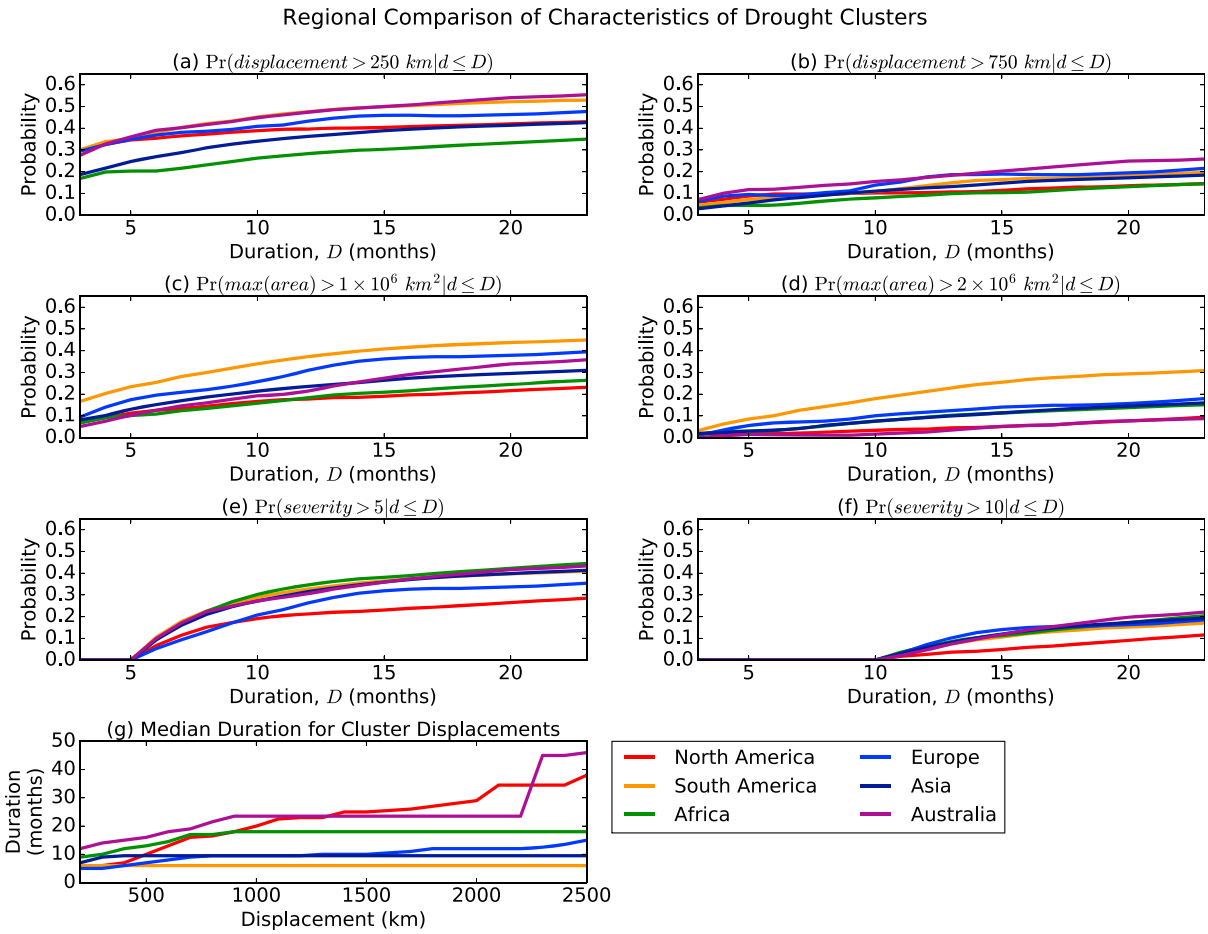

Figure 2. CCDFs of (a and b) displacements, (c and d) maximum areas, and (e and f) severities exceeding two thresholds, conditional on a range of durations, for each region. (g) Median duration of clusters that have reached a range of displacements in each region.

severity thresholds, except for North America, where droughts tend to be less severe, comparatively. Figure 2g shows the median durations that it took clusters to reach a range of displacements. They suggest that South American and Asian clusters tend to have faster displacements, and African and Australian clusters slower ones. This shows that although droughts appear to displace everywhere in the world, there are distinct regional differences in their behaviors month-to-month.

Monthly rates of change of area and mean intensity were calculated for clusters of different areas and mean intensities, respectively. Figure 3 shows the resulting 2-D histograms and linear regressions. The high frequencies in the 2-D histogram for smaller areas imply that smaller clusters (that are still larger than 200,000 km^2) have a higher propensity of growing further. Conversely, very large clusters located in the middle and right end of the *x* axis tend to shrink instead. The histograms of the clusters' intensities show higher frequencies of positive changes for less intense droughts (that have reached dry anomaly of the 15th percentile) and higher frequencies of negative changes for more intense droughts. This implies that less intense droughts tend to intensify further. The negative correlations from the linear regressions support these conclusions. The dynamics shown here may be partially due to local positive feedbacks (e.g., precipitation recycling) that lock clusters into drought conditions making it harder for recovery to take place [e.g., *Giannini et al.*, 2003; *Wu and Kinter*, 2009; *D'Odorico et al.*, 2013; *Roundy et al.*, 2013].

3.3. Role of Moisture Exports Reduction on Drought Propagation

Disjoint domains from the same clusters were used to identify regions that are atmospherically connected and to study the contributions of anomalies of moisture exports on drought propagation. Figure 4a shows

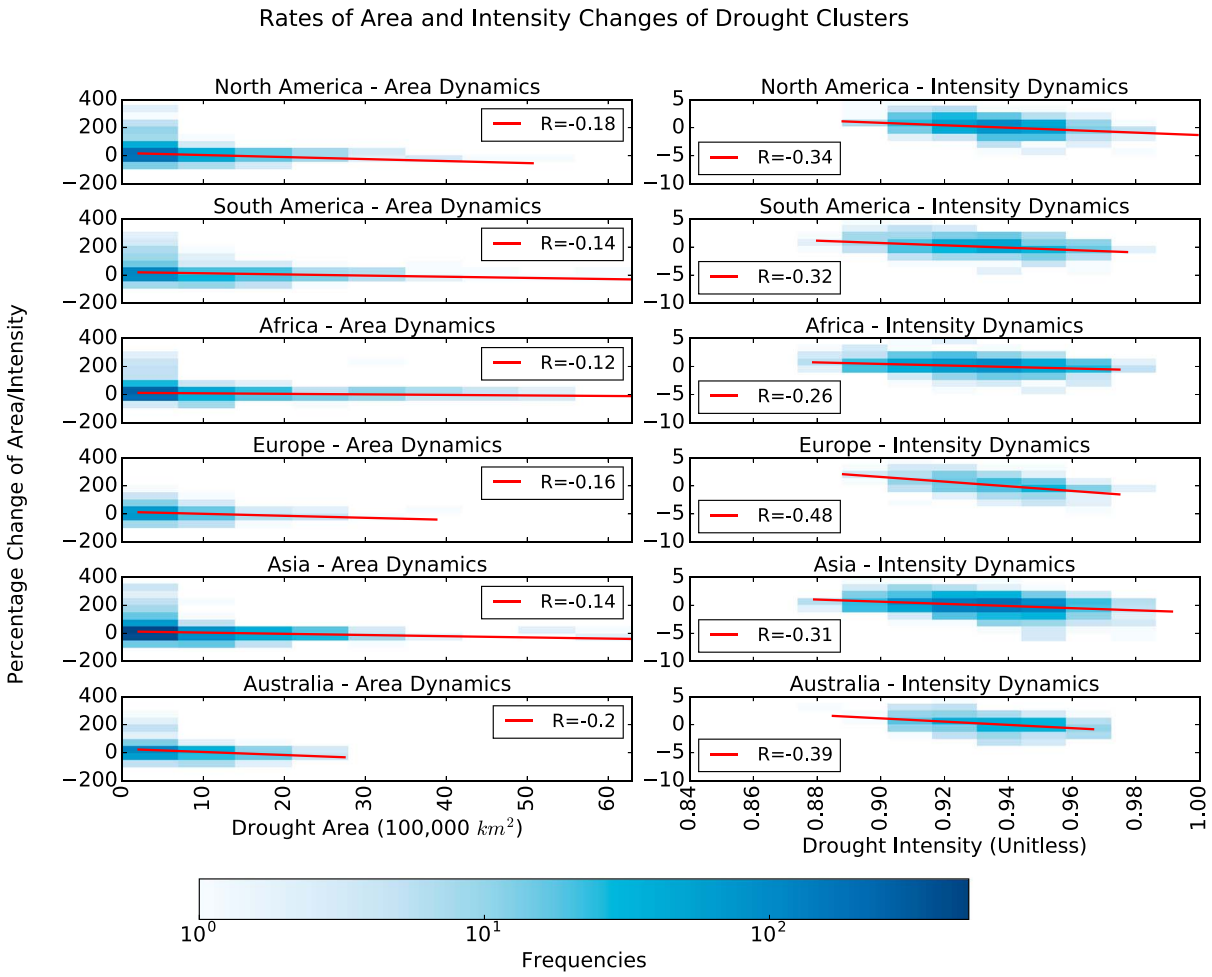

Figure 3. Regional 2-D histograms of rates of change in (left column) area and (right column) intensity as a function of area and intensity, respectively, during the previous month. Red line displays linear regression results. All correlations yielded $p < 0.05$.

example domains R1 and R2 as described in section 2.4 for the cluster in Figure 1a. Figure 4b displays the scatterplot and Spearman's ρ between the monthly time series (1979–2009) of ET anomalies averaged over R1 and the MF anomalies across the boundary in the direction of R2 in Figure 4a. Similarly, Figure 4c shows the relationship between MF anomalies across the boundary and Prcp anomalies averaged over R2. Since these two correlations were positive and significant, and the mean flux across the boundary toward R2 was positive (not shown), we conclude that reduction of moisture exports from R1 can influence drought propagation into R2 for this pair of domains.

This analysis was repeated for 60 pairs of disjoint domains in total, globally, and R2 was determined to be downwind from R1 in 42 of them. Figure 4d shows the histograms of Spearman ρ's between ET anomalies and MF anomalies for those 42 cases, and Figure 4e the Spearman ρ's between MF anomalies and Prcp anomalies. The shaded red bars correspond to the cases for which moisture exports were found to have made a contribution to drought propagation as defined above. Figure 4f displays the percentage of domain pairs for which reduction of moisture exports was found to be a contributing factor for drought propagation in each region, including all pairs. North and South America had the highest proportion (45% and 27%, respectively), while Australia and Asia had the lowest (0% and 10%, respectively). These results suggest that regional land-atmospheric feedbacks may play a role in drought propagation at the large, subcontinental spatial scales considered in this study, though other atmospheric mechanisms are also important. This is a first-order analysis that considers predominant MF at the monthly scale, but further work should be done using MF derived at higher temporal resolutions.

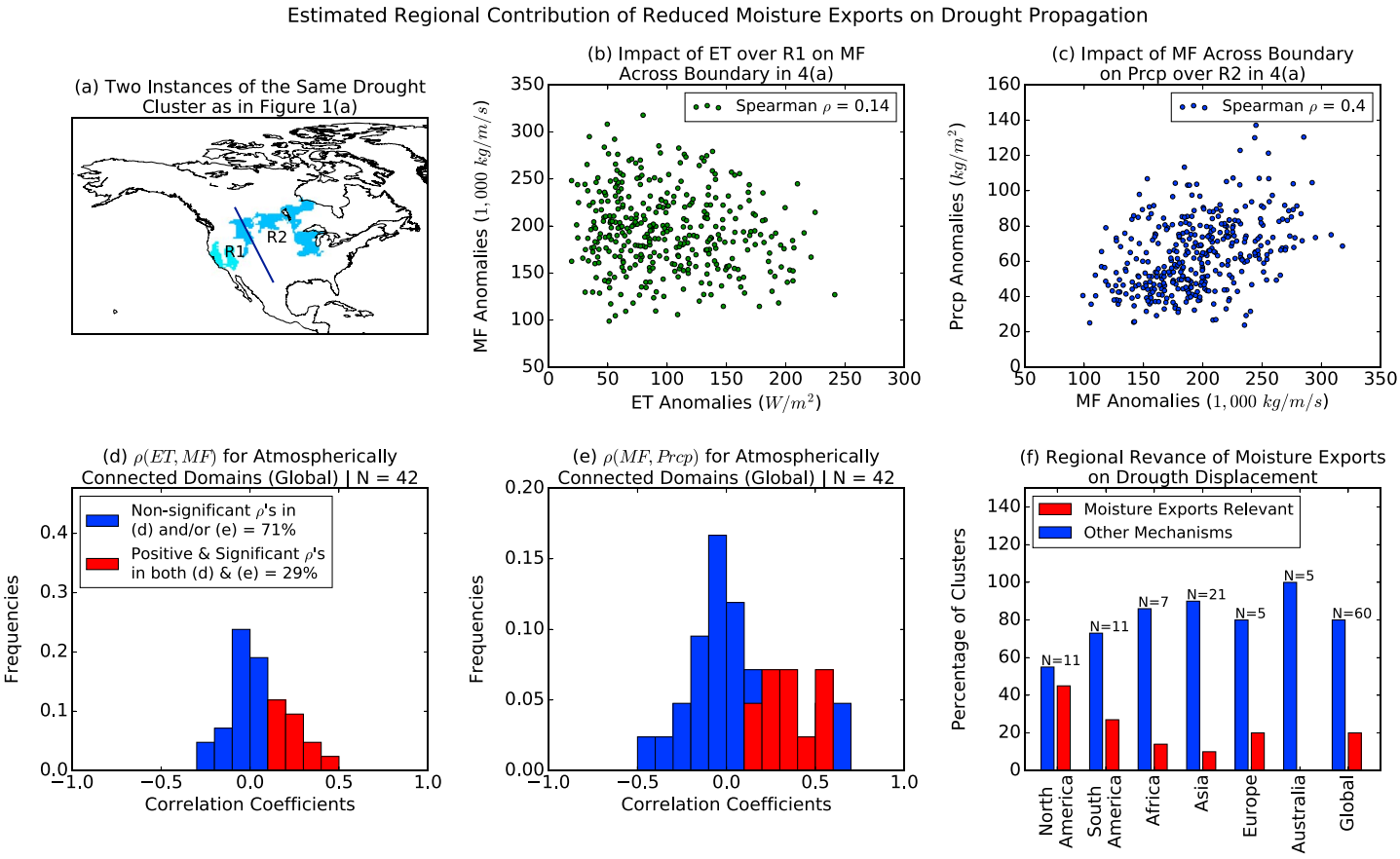

Figure 4. (a) Example of domains R1, R2, and the boundary between them. (b) Scatterplot and ρ between ET anomalies over R1 and MF across the boundary toward R2 shown in Figure 4a. (c) Similar to Figure 4b for MF anomalies across the boundary and Prcp anomalies over R2. (d and e) Histograms of ρ's between ET and MF, and between MF and Prcp, respectively, for atmospherically connected domains. (f) Percentages of cases where the pair of correlations was positive and significant in each region.

4. Discussion and Conclusions

CFSR data were used here to identify drought clusters and characterize their monthly spatiotemporal dynamics across the world. This work advances our current understanding of drought dynamics, showing that drought clusters can displace hundreds of kilometers in every continent, sometimes partially due to the reduction of moisture exports that propagate the drought signal downwind. While these traveling droughts might only represent a small fraction of the total number of events, they are likely to have some of the largest societal impacts given that they are also the longest lasting and most severe ones.

This analysis draws a parallel with tropical cyclone studies, in which the densities and directions of their tracks have been analyzed in the world's oceans [*Zhao et al.*, 2009]. Similarly, there are hotspots where more droughts pass through and common directions that they tend to follow over various land-regions around the world.

The drought clusters' displacements and their area and intensity dynamics suggest that land-atmospheric feedback mechanisms, such as precipitation recycling, might play an important role in the evolution of droughts, both locally and downwind [e.g., *Dominguez et al.*, 2009; *Roundy et al.*, 2013]. This is in addition to other atmospheric phenomena, such as the displacement of high-pressure systems, and heightened probability of drought over large areas due to teleconnections with sea surface temperatures. Results shown here also suggest the existence of area and intensity thresholds beyond which it is more likely for droughts to grow and intensify before they recover.

Improved understanding of the physical mechanisms behind the spatiotemporal dynamics of droughts explored here highlights areas in which forecast models should be improved. Combining the approach

presented in this work with increased understanding of the physical mechanisms may enable the development of statistical-physical models of drought clusters that can be used for risk assessment and seasonal forecasting, similar to those for tropical cyclones [e.g., *Yonekura and Hall*, 2011].

The ability of droughts to displace across regions also poses important implications for regional cooperation and information exchange between governments at different scales (e.g., municipal, state, and national) regarding drought risk mitigation and management. An example of this is the North American Drought Monitor, which links information between Mexico, the U.S., and Canada [*Lawrimore et al*., 2002]. These information systems can help stakeholders make appropriate decisions to mitigate droughts' impacts before they displace into their region and throughout the droughts' development.

Acknowledgments
The authors wish to thank the members of the Terrestrial Hydrology Research Group at Princeton University, the members of the Water Program at the International Institute of Applied Systems Analysis (IIASA), and two anonymous reviewers for their comments, which helped improve this study. Sections of this work were carried out as part of the Young Scientists and Scholars Program at IIASA. This research was funded by the NASA Earth and Space Science Fellowship, grant NNX14AL08H S02, and NOAA, grant NA14OAR4310218. CFSR data used here are available at http://rda.ucar.edu.

References

Andreadis, K. M., E. A. Clark, A. W. Wood, A. F. Hamlet, and D. P. Lettenmaier (2005), Twentieth-century drought in the conterminous United States, *J. Hydrometeorol.*, *6*(6), 985–1001, doi:10.1175/JHM450.1.

Arnault, J., R. Knoche, J. Wei, and H. Kunstmann (2016), Evaporation tagging and atmospheric water budget analysis with WRF: A regional precipitation recycling study for West Africa, *Water Resour. Res.*, *52*(3), 1544–1567, doi:10.1002/2015WR017704.

D'Odorico, P., A. Bhattachan, K. F. Davis, S. Ravi, and C. W. Runyan (2013), Global desertification: Drivers and feedbacks, *Adv. Water Resour.*, *51*, 326–344, doi:10.1016/j.advwatres.2012.01.013.

Dominguez, F., J. C. Villegas, and D. D. Breshears (2009), Spatial extent of the North American Monsoon: Increased cross-regional linkages via atmospheric pathways, *Geophys. Res. Lett.*, *36*, L07401, doi:10.1029/2008GL037012.

Eltahir, E. A. B., and R. L. Bras (1996), Precipitation recycling, *Rev. Geophys.*, *34*(3), 367–378, doi:10.1029/96RG01927.

Ge, Y., T. Apurv, and X. Cai (2016), Spatial and temporal patterns of drought in the Continental U.S. during the past century, *Geophys. Res. Lett.*, *43*, doi:10.1002/2016GL069660.

Giannini, A., R. Saravanan, and P. Chang (2003), Oceanic forcing of Sahel rainfall on interannual to interdecadal time scales, *Science*, *302*(5647), 1027–1030, doi:10.1126/science.1089357.

Gocic, M., and S. Trajkovic (2014), Spatiotemporal characteristics of drought in Serbia, *J. Hydrol.*, *510*, 110–123, doi:10.1016/j.jhydrol.2013.12.030.

Guttman, N. B. (1999), Accepting the standardized precipitation index: A calculation algorithm, *J. Am. Water Resour. Assoc.*, *35*(2), 311–322, doi:10.1111/j.1752-1688.1999.tb03592.x.

Hoerling, M., J. Eischeid, A. Kumar, R. Leung, A. Mariotti, K. Mo, S. Schubert, and R. Seager (2014), Causes and predictability of the 2012 Great Plains drought, *Bull. Am. Meteorol. Soc.*, *95*(2), 269–282, doi:10.1175/BAMS-D-13-00055.1.

Kam, J., J. Sheffield, X. Yuan, and E. F. Wood (2013), The influence of Atlantic tropical cyclones on drought over the eastern United States (1980–2007), *J. Clim.*, *26*(10), 3067–3086, doi:10.1175/JCLI-D-12-00244.1.

Keys, P. W., E. A. Barnes, R. J. van der Ent, and L. J. Gordon (2014), Variability of moisture recycling using a precipitationshed framework, *Hydrol. Earth Syst. Sci.*, *18*(10), 3937–3950, doi:10.5194/hess-18-3937-2014.

Lawrimore, J., R. R. Heim, M. Svoboda, V. Swail, and P. J. Englehart (2002), Beginning a new era of drought monitoring across North America, *Bull. Am. Meteorol. Soc.*, *83*(8), 1191–1192, doi:10.1175/1520-0477(2002)083<1191:BANEOD>2.3.CO;2.

Lloyd-Hughes, B. (2012), A spatio-temporal structure-based approach to drought characterisation, *Int. J. Climatol.*, *32*(3), 406–418, doi:10.1002/joc.2280.

Meng, J., R. Yang, H. Wei, M. Ek, G. Gayno, P. Xie, and K. Mitchell (2012), The land surface analysis in the NCEP Climate Forecast System Reanalysis, *J. Hydrometeorol.*, *13*(5), 1621–1630, doi:10.1175/JHM-D-11-090.1.

Mishra, A. K., and V. P. Singh (2011), Drought modeling—A review, *J. Hydrol.*, *403*(1-2), 157–175, doi:10.1016/j.jhydrol.2011.03.049.

Mo, K. C., and J. E. Schemm (2008), Droughts and persistent wet spells over the United States and Mexico, *J. Clim.*, *21*(5), 980–994, doi:10.1175/2007JCLI1616.1.

Mo, K. C., L. N. Long, Y. Xia, S. K. Yang, J. E. Schemm, and M. Ek (2011), Drought indices based on the climate forecast system reanalysis and ensemble NLDAS, *J. Hydrometeorol.*, *12*(2), 181–205, doi:10.1175/2010JHM1310.1.

Rajagopalan, B., E. Cook, U. Lall, and B. K. Ray (2000), Spatiotemporal variability of ENSO and SST teleconnections to summer drought over the United States during the twentieth century, *J. Clim.*, *13*(24), 4244–4255, doi:10.1175/1520-0442(2000)013<4244:SVOEAS>2.0.CO;2.

Rodriguez-Iturbe, I., D. Entekhabi, and R. L. Bras (1991a), Nonlinear dynamics of soil moisture at climate scales: 1. Stochastic analysis, *Water Resour. Res.*, *27*(8), 1899–1906, doi:10.1029/91WR01035.

Rodriguez-Iturbe, I., D. Entekhabi, J.-S. Lee, and R. L. Bras (1991b), Nonlinear dynamics of soil moisture at climate scales: 2. Chaotic analysis, *Water Resour. Res.*, *27*(8), 1907–1915, doi:10.1029/91WR01036.

Roundy, J. K., C. R. Ferguson, and E. F. Wood (2013), Temporal variability of land-atmosphere coupling and its implications for drought over the southeast United States, *J. Hydrometeorol.*, *14*(2), 622–635, doi:10.1175/JHM-D-12-090.1.

Seneviratne, S. I., T. Corti, E. L. Davin, M. Hirschi, E. B. Jaeger, I. Lehner, B. Orlowsky, and A. J. Teuling (2010), Investigating soil moisture-climate interactions in a changing climate: A review, *Earth Sci. Rev.*, *99*(3-4), 125–161, doi:10.1016/j.earscirev.2010.02.004.

Shabbar, A., and W. Skinner (2004), Summer drought patterns in Canada and the relationship to global sea surface temperatures, *J. Clim.*, *17*(14), 2866–2880, doi:10.1175/1520-0442(2004)017<2866:SDPICA>2.0.CO;2.

Sheffield, J., and E. F. Wood (2011), *Drought: Past Problems and Future Scenarios*, Earthscan, Print, London.

Sheffield, J., K. M. Andreadis, E. F. Wood, and D. P. Lettenmaier (2009), Global and continental drought in the second half of the twentieth century: Severity–area–duration analysis and temporal variability of large-scale events, *J. Clim.*, *22*(8), 1962–1981, doi:10.1175/2008JCLI2722.1.

Szép, I. J., J. Mika, and Z. Dunkel (2005), Palmer drought severity index as soil moisture indicator: Physical interpretation, statistical behaviour and relation to global climate, *Phys. Chem. Earth, Parts A/B/C*, *30*(1-3), 231–243, doi:10.1016/j.pce.2004.08.039.

Tallaksen, L. M., and K. Stahl (2014), Spatial and temporal patterns of large-scale droughts in Europe: Model dispersion and performance, *Geophys. Res. Lett.*, *41*, 429–434, doi:10.1002/2013GL058573.

Vicente-Serrano, S. M. (2006), Differences in spatial patterns of drought on different time scales: An analysis of the Iberian Peninsula, *Water Resour. Manage.*, *20*(1), 37–60, doi:10.1007/s11269-006-2974-8.

Vidal, J.-P., E. Martin, L. Franchistéguy, F. Habets, J.-M. Soubeyroux, M. Blanchard, and M. Baillon (2010), Multilevel and multiscale drought reanalysis over France with the Safran-Isba-Modcou hydrometeorological suite, *Hydrol. Earth Syst. Sci.*, *14*(3), 459–478, doi:10.5194/hess-14-459-2010.

Wang, K., Q. Li, Y. Yang, M. Zeng, P. Li, and J. Zhang (2015), Analysis of spatio-temporal evolution of droughts in Luanhe River Basin using different drought indices, *Water Sci. Eng.*, *8*(4), 282–290, doi:10.1016/j.wse.2015.11.004.

Wood, E. F., S. D. Schubert, A. W. Wood, C. D. Peters-Lidard, K. C. Mo, A. Mariotti, and R. S. Pulwarty (2015), Prospects for advancing drought understanding, monitoring, and prediction, *J. Hydrometeorol.*, *16*(4), 1636–1657, doi:10.1175/JHM-D-14-0164.1.

World Bank (2012), *Food Price Watch – August 2012*, The World Bank, Washington, D. C.

Wu, R., and J. L. Kinter (2009), Analysis of the relationship of U.S. droughts with SST and soil moisture: Distinguishing the time scale of droughts, *J. Clim.*, *22*(17), 4520–4538, doi:10.1175/2009JCLI2841.1.

Xu, K., D. Yang, H. Yang, Z. Li, Y. Qin, and Y. Shen (2015), Spatio-temporal variation of drought in China during 1961–2012: A climatic perspective, *J. Hydrol.*, *526*, 253–264, doi:10.1016/j.jhydrol.2014.09.047.

Yonekura, E., and T. M. Hall (2011), A statistical model of tropical cyclone tracks in the western North Pacific with ENSO-dependent cyclogenesis, *J. Appl. Meteorol. Climatol.*, *50*(8), 1725–1739, doi:10.1175/2011JAMC2617.1.

Zhai, J., J. Huang, B. Su, L. Cao, Y. Wang, T. Jiang, and T. Fischer (2016), Intensity–area–duration analysis of droughts in China 1960–2013, *Clim. Dyn.*, 1–18, doi:10.1007/s00382-016-3066-y.

Zhan, W., K. Guan, J. Sheffield, and E. F. Wood (2016), Depiction of drought over sub-Saharan Africa using reanalyses precipitation data sets, *J. Geophys. Res. Atmos.*, *121*, 10,555–10,574, doi:10.1002/2016JD024858.

Zhao, M., I. M. Held, S.-J. Lin, and G. A. Vecchi (2009), Simulations of global hurricane climatology, interannual variability, and response to global warming using a 50-km resolution GCM, *J. Clim.*, *22*(24), 6653–6678, doi:10.1175/2009JCLI3049.1.